Research Article | Vol. 8, No. 2 | 1 Feb 2017 | BIOMEDICAL OPTICS EXPRESS 860
Biomedical Optics EXPRESS

Detecting ordered small molecule drug aggregates in live macrophages: a multi-parameter microscope image data acquisition and analysis strategy

PHILLIP RZECZYCKI,[1] GI SANG YOON,[1] RAHUL K. KESWANI,[1] SUDHA SUD,[1] KATHLEEN A. STRINGER,[2] AND GUS R. ROSANIA[1,*]

[1]*Department of Pharmaceutical Sciences, University of Michigan College of Pharmacy, 428 Church Street, Ann Arbor, MI 48109, USA*
[2]*Department of Clinical Pharmacy, University of Michigan College of Pharmacy, 428 Church Street, Ann Arbor, MI 48109, USA*
[*]*grosania@umich.edu*

Abstract: Following prolonged administration, certain orally bioavailable but poorly soluble small molecule drugs are prone to precipitate out and form crystal-like drug inclusions (CLDIs) within the cells of living organisms. In this research, we present a quantitative multi-parameter imaging platform for measuring the fluorescence and polarization diattenuation signals of cells harboring intracellular CLDIs. To validate the imaging system, the FDA-approved drug clofazimine (CFZ) was used as a model compound. Our results demonstrated that a quantitative multi-parameter microscopy image analysis platform can be used to study drug sequestering macrophages, and to detect the formation of ordered molecular aggregates formed by poorly soluble small molecule drugs in animals.

OCIS codes: (260.5430) Polarization; (170.1530) Cell analysis; (170.3880) Medical and biological imaging; (170.0110) Imaging systems.

References and links

1. C. J. Hewitt and G. Nebe-Von-Caron, "The application of multi-parameter flow cytometry to monitor individual microbial cell physiological state," Adv. Biochem. Eng. Biotechnol. **89**, 197–223 (2004).
2. G. S. Kaminski Schierle, M. Sauer, and C. F. Kaminski, "Chapter 10 - Probing Amyloid Aggregation and Morphology In Situ by Multiparameter Imaging and Super-Resolution Fluorescence Microscopy," in *Bio-nanoimaging*, V. N. U. L. Lyubchenko, ed. (Academic Press, Boston, 2014), pp. 105–120.
3. S. B. Sparenga, "The Importance of Polarized Light Microscopy in the Analytical Setting," Microsc. Microanal. **14**(S2), 1032–1033 (2008).
4. S. B. Mehta, M. Shribak, and R. Oldenbourg, "Polarized light imaging of birefringence and diattenuation at high resolution and high sensitivity," J. Opt. **15**(9), 094007 (2013).
5. R. Oldenbourg, "Polarization state generated by universal polarizer" (2013), retrieved 8 May, 2015, openpolscope.org/pages/PolarizationEllipseUniversalPolarizer.htm.
6. R. Oldenbourg, "Polarized Light Microscopy: Principles and Practice," Cold Spring Harbor Protocols 2013, pdb.top078600 (2013).
7. W. Kaminsky, K. Claborn, and B. Kahr, "Polarimetric imaging of crystals," Chem. Soc. Rev. **33**(8), 514–525 (2004).
8. W. Kaminsky, E. Gunn, R. Sours, and B. Kahr, "Simultaneous false-colour imaging of birefringence, extinction and transmittance at camera speed," J. Microsc. **228**(2), 153–164 (2007).
9. C. A. Valades Cruz, H. A. Shaban, A. Kress, N. Bertaux, S. Monneret, M. Mavrakis, J. Savatier, and S. Brasselet, "Quantitative nanoscale imaging of orientational order in biological filaments by polarized superresolution microscopy," Proc. Natl. Acad. Sci. U.S.A. **113**(7), E820–E828 (2016).
10. R. Turcotte, J. M. Mattson, J. W. Wu, Y. Zhang, and C. P. Lin, "Molecular Order of Arterial Collagen Using Circular Polarization Second-Harmonic Generation Imaging," Biophys. J. **110**(3), 530–533 (2016).
11. B. C. Vidal, E. H. M. Dos Anjos, and M. L. S. Mello, "Optical anisotropy reveals molecular order in a mouse enthesis," Cell Tissue Res. **362**(1), 177–185 (2015).
12. J. A. Byrne, D. A. Pedersen, L. L. Clepper, M. Nelson, W. G. Sanger, S. Gokhale, D. P. Wolf, and S. M. Mitalipov, "Producing primate embryonic stem cells by somatic cell nuclear transfer," Nature **450**(7169), 497–502 (2007).

#282276 http://dx.doi.org/10.1364/BOE.8.000860
Journal © 2017 Received 7 Dec 2016; accepted 10 Jan 2017; published 13 Jan 2017

Biomedical Optics EXPRESS

13. L. Liu, R. Oldenbourg, J. R. Trimarchi, and D. L. Keefe, "A reliable, noninvasive technique for spindle imaging and enucleation of mammalian oocytes," Nat. Biotechnol. **18**(2), 223–225 (2000).
14. P. A. A. S. Navarro, L. Liu, J. R. Trimarchi, R. A. Ferriani, and D. L. Keefe, "Noninvasive imaging of spindle dynamics during mammalian oocyte activation," Fertil. Steril. **83**(4 Suppl 1), 1197–1205 (2005).
15. B. S. DeMay, X. Bai, L. Howard, P. Occhipinti, R. A. Meseroll, E. T. Spiliotis, R. Oldenbourg, and A. S. Gladfelter, "Septin filaments exhibit a dynamic, paired organization that is conserved from yeast to mammals," J. Cell Biol. **193**(6), 1065–1081 (2011).
16. R. Oldenbourg, E. D. Salmon, and P. T. Tran, "Birefringence of Single and Bundled Microtubules," Biophys. J. **74**(1), 645–654 (1998).
17. W. Kaminksy, L.-W. Jin, S. Powell, I. Maezawa, K. Claborn, C. Branham, and B. Kahr, "Polarimetric imaging of amyloid," Micron **37**(4), 324–338 (2006).
18. J. Baik and G. R. Rosania, "Macrophages Sequester Clofazimine in an Intracellular Liquid Crystal-Like Supramolecular Organization," PLoS One **7**(10), e47494 (2012).
19. J. Baik and G. R. Rosania, "Molecular imaging of intracellular drug-membrane aggregate formation," Mol. Pharm. **8**(5), 1742–1749 (2011).
20. R. Keswani, G. Yoon, S. Sud, K. Stringer, and G. Rosania, "A Far-Red Fluorescent Probe For Flow Cytometric Xenobiotic-Sequestering Cell Functional Studies," Cytometry A **87**(9), 855–867 (2015).
21. G. S. Yoon, S. Sud, R. K. Keswani, J. Baik, T. J. Standiford, K. A. Stringer, and G. R. Rosania, "Phagocytosed Clofazimine Biocrystals Can Modulate Innate Immune Signaling by Inhibiting TNFα and Boosting IL-1RA Secretion," Mol. Pharm. **12**(7), 2517–2527 (2015).
22. A. Edelstein, N. Amodaj, K. Hoover, R. Vale, and N. Stuurman, "Computer Control of Microscopes Using μManager," in *Current Protocols in Molecular Biology,* (John Wiley & Sons, Inc., 2010).
23. R. Oldenbourg, "Diattenuation" (2013), retrieved May 8 2015, openpolscope.org/pages/Diattenuation.htm.
24. M. D. Abramoff, P. J. Magalhaes, and S. J. Ram, "Image Processing With ImageJ," Biophoton. Int. **11**, 36–42 (2004).
25. T. Ferreira and W. Rasband, "ImageJ User Guide," (FIJI, rsbweb.nih.gov, 2012).
26. C. A. Schneider, W. S. Rasband, and K. W. Eliceiri, "NIH Image to ImageJ: 25 years of image analysis," Nat. Methods **9**(7), 671–675 (2012).
27. J. Baik, K. A. Stringer, G. Mane, and G. R. Rosania, "Multiscale Distribution and Bioaccumulation Analysis of Clofazimine Reveals a Massive Immune System-Mediated Xenobiotic Sequestration Response," Antimicrob. Agents Chemother. **57**(3), 1218–1230 (2013).
28. G. S. Yoon, S. Sud, R. K. Keswani, J. Baik, T. J. Standiford, K. A. Stringer, and G. R. Rosania, "Phagocytosed Clofazimine Biocrystals Can Modulate Innate Immune Signaling by Inhibiting TNFα and Boosting IL-1RA Secretion," Mol. Pharm. **12**(7), 2517–2527 (2015).
29. G. S. Yoon, R. K. Keswani, S. Sud, P. M. Rzeczycki, M. D. Murashov, T. A. Koehn, T. J. Standiford, K. A. Stringer, and G. R. Rosania, "Clofazimine Biocrystal Accumulation in Macrophages Upregulates IL-1RA Production to Induce a Systemic Anti-Inflammatory State," Antimicrob. Agents Chemother. **60**(6), 3470–3479 (2016).
30. L. D. Loose, J. B. Silkworth, T. Charbonneau, and F. Blumenstock, "Environmental chemical-induced macrophage dysfunction," Environ. Health Perspect. **39**, 79–91 (1981).
31. S. Inoué, "Polarization Microscopy," in *Current Protocols in Cell Biology* (John Wiley & Sons, Inc., 2002), p. 27.
32. F. Massoumian, R. Juskaitis, M. A. A. Neil, and T. Wilson, "Quantitative polarized light microscopy," J. Microsc. **209**(1), 13–22 (2003).
33. K. A. Min, W. G. Rajeswaran, R. Oldenbourg, G. Harris, R. K. Keswani, M. Chiang, P. Rzeczycki, A. Talattof, M. Hafeez, R. W. Horobin, S. D. Larsen, K. A. Stringer, and G. R. Rosania, "Massive Bioaccumulation and Self-Assembly of Phenazine Compounds in Live Cells," Adv Sci (Weinh) **2**(8), 1500025 (2015).
34. R. K. Keswani, J. Baik, L. Yeomans, C. Hitzman, A. M. Johnson, A. S. Pawate, P. J. Kenis, N. Rodriguez-Hornedo, K. A. Stringer, and G. R. Rosania, "Chemical Analysis of Drug Biocrystals: A Role for Counterion Transport Pathways in Intracellular Drug Disposition," Mol. Pharm. **12**(7), 2528–2536 (2015).
35. R. S. Funk and J. P. Krise, "Cationic amphiphilic drugs cause a marked expansion of apparent lysosomal volume: implications for an intracellular distribution-based drug interaction," Mol. Pharm. **9**(5), 1384–1395 (2012).
36. R. Logan, A. C. Kong, and J. P. Krise, "Time-Dependent Effects of Hydrophobic Amine-Containing Drugs on Lysosome Structure and Biogenesis in Cultured Human Fibroblasts," J. Pharm. Sci. **103**(10), 3287–3296 (2014).
37. H. J. Zimmerman, *Hepatotoxicity: The Adverse Effects of Drugs and Other Chemicals on the Liver* (Lippincott Williams & Wilkins, 1999).
38. C. A. Naughton, "Drug-induced nephrotoxicity," Am. Fam. Physician **78**(6), 743–750 (2008).
39. S. L. Ciesla, J. Trahan, W. B. Wan, J. R. Beadle, K. A. Aldern, G. R. Painter, and K. Y. Hostetler, "Esterification of cidofovir with alkoxyalkanols increases oral bioavailability and diminishes drug accumulation in kidney," Antiviral Res. **59**(3), 163–171 (2003).
40. S. R. Hawley, P. G. Bray, M. Mungthin, J. D. Atkinson, P. M. O'Neill, and S. A. Ward, "Relationship between antimalarial drug activity, accumulation, and inhibition of heme polymerization in Plasmodium falciparum in vitro," Antimicrob. Agents Chemother. **42**(3), 682–686 (1998).

Biomedical Optics EXPRESS

41. S. R. Hawley, P. G. Bray, P. M. O'Neill, B. K. Park, and S. A. Ward, "The role of drug accumulation in 4-aminoquinoline antimalarial potency," Biochem. Pharmacol. **52**(5), 723–733 (1996).
42. W. Mickols, M. F. Maestre, I. Tinoco, Jr., and S. H. Embury, "Visualization of oriented hemoglobin S in individual erythrocytes by differential extinction of polarized light," Proc. Natl. Acad. Sci. U.S.A. **82**(19), 6527–6531 (1985).
43. P. Libby, "Molecular and cellular mechanisms of the thrombotic complications of atherosclerosis," J. Lipid Res. **50**(Suppl), S352–S357 (2008).
44. J. R. Molano and V. Molano, "Dementia with Lewy bodies," Semin. Neurol. **33**(4), 330–335 (2013).
45. H. Z. Amin, S. Mori, N. Sasaki, and K. Hirata, "Diagnostic Approach to Cardiac Amyloidosis," Kobe J. Med. Sci. **60**(1), E5–E11 (2014).
46. M. Biegstraaten, G. E. Linthorst, I. N. van Schaik, and C. E. M. Hollak, "Fabry Disease: a Rare Cause of Neuropathic Pain," Curr. Pain Headache Rep. **17**(10), 365 (2013).

1. Introduction

For studying complex cell populations, fluorescence-based multi-parameter cytometric analysis techniques are routinely used for monitoring the expression of multiple phenotypic markers at a single cell level. For this purpose, fluorescence-based flow and image cytometry instruments can be used to quantify the expression of different molecular markers down to the level of individual cells, using fluorescently tagged antibodies that recognize specific cell surface receptors, intracellular proteins or other cellular targets of interest. These antibodies are labeled with fluorophores that are excited and emit light specific wavelengths, allowing for simultaneous detection of multiple different fluorescence signals at different excitation and emission wavelengths [1].

While many multi-parameter, cytometric analysis instruments are available for analyzing samples based on a single optical modality (e.g. fluorescence), the development of multi-parameter imaging platforms for phenotypic analysis of cell populations based on various optical properties (e.g. fluorescence, transmittance, and birefringence) is an emerging area of research. For example, the combination of polarization, transmittance and fluorescence imaging modalities could be useful to study protein aggregation at a single cell level [2].

Indeed, the ability to combine fluorescence, transmittance, and polarization microscopy measurements could be useful in obtaining new insights into the organization of molecules in biological specimens [3]. Similar to conventional, transmitted light microscopy, polarization microscopy instruments can employ polarized, transmitted light to study the structure of supramolecular aggregates within individual cells [4–7]. Because of the manner in which polarized light interacts with ordered molecular structures, differences in the organization of molecular components can be detected and quantified based on the fraction of light that is transmitted through the material when it is illuminated with polarized light [8]. At the simplest level, the diattenuation anisotropy of a material can be measured as the maximal difference in light transmittance of a perpendicular pair of planes of polarized light passing through a material, as the material is rotated in the direction perpendicular to both polarized planes of light. These measurements allow distinguishing between homogenous and heterogeneous materials comprised of subdomains of molecules arranged in a particular direction. Polarization microscopy can also be used to obtain information about how the molecules within these subdomains are oriented, providing insight into the underlying molecular order of the material [9–11].

Previously, polarization microscopy has been used extensively to image ordered supramolecular structures in live cells [12–16], as well as to study the formation of intracellular aggregates [17]. This led us to consider combining quantitative polarization microscopy together with fluorescence and transmittance measurements to facilitate multi-parameter cytometric analysis of molecular aggregates formation at a single cell level.

Here, we present a multi-parameter imaging instrument and analysis platform for the analysis of live cell populations, at a single cell level. For demonstration purposes, we used this imaging platform to study the formation of intracellular crystal-like drug inclusions (CLDIs) formed by clofazimine (CFZ) -an FDA-approved drug that accumulates as highly

Biomedical Optics EXPRESS

ordered supramolecular aggregates in macrophages of drug-treated mice [18,19]. In flow cytometric experiments, CLDIs have been shown to exhibit a strong signal in the Cy5 fluorescence range (650 nm excitation/670 nm emission) [20]. Taking advantage of this intrinsic fluorescence of these biocrystals, we proceeded to analyze the optical anisotropy and fluorescent properties of live cells containing CLDIs, and probe for any relationship between these properties within cells. Our results demonstrate how this multi-parameter imaging platform can be used to study drug accumulation and detect ordered aggregates within live-cells.

2. Materials and methods

2.1 Clofazimine administration to mice

Mice (4 week old, male C57Bl6) were purchased from the Jackson Laboratory (Bar Harbor, ME) and acclimatized for 1 week in a specific-pathogen-free animal facility. Clofazimine (CFZ) (C8895; Sigma, St. Louis, MO) was dissolved in sesame oil (Roland, China, or Shirakiku, Japan) to achieve a concentration of 3 mg/ml, which was mixed with Powdered Lab Diet 5001 (PMI International, Inc., St. Louis, MO) to produce a 0.03% drug to powdered feed mix, and orally administered *ad libitum* for 8 weeks. A corresponding amount of sesame oil was mixed with chow for vehicle treatment (control). Animal care was provided by the University of Michigan's Unit for Laboratory Animal Medicine (ULAM), and the experimental protocol was approved by the Committee on Use and Care of Animals (Protocol PRO00005542).

2.2 Isolation of spleen CLDIs

CLDIs were isolated from the spleen of 8 week CFZ fed mice using a previously described method [21]. In brief, the spleens were homogenized with a syringe plunger and then filtered through a 40 μm cell strainer to remove connective tissue debris. The spleen filtrate was centrifuged (300 *x* g for 10 min) to remove large cell debris and the pelleted CLDIs were resuspended in 10% sucrose in Dulbecco's PBS (DPBS; Life Technologies, Carlsbad, CA) without $CaCl_2$ and $MgCl_2$, pH 7.4. CLDIs were further purified using a 3-layer discontinuous gradient (50%, 30% and 10% sucrose in DPBS) centrifugation method (3200 ^{x} g for 30 min).

2.3 Isolation of alveolar macrophages

CFZ or control chow-fed mice (n = 3 per group) were euthanized by carbon dioxide asphyxiation followed by exsanguination. The trachea was surgically exposed and cannulated with an 18G needle and the lungs were lavaged by instilling DPBS containing 0.5 mM EDTA (Sigma) in 1 ml aliquots for a total of 6 ml. Approximately 90% of the bronchoalveolar lavage (BAL) was retrieved. BAL was then centrifuged for 10 min at 400 x g, 4°C, resuspended in RPMI 1640 media (Life Technologies) and the cells were pooled together. The cells were then plated onto 4 or 8 chamber coverglass (#1.5, Lab-Tek II, Nunc, Rochester, NY) for imaging studies. The cells were allowed to attach for 45 min and then washed with media, enabling the isolation of alveolar macrophages by adherence.

2.4 Multi-parameter imaging instrument set up

The multi-parameter imaging instrument utilized by our laboratory combines three imaging separate imaging modalities onto a single instrument, allowing for the fluorescence, transmittance, and polarization properties of a sample to be rapidly acquired. Polarization measurements are acquired utilizing the diattenuation LC-PolScope microscope, a custom built microscopic imaging system similar to the birefringence LC-PolScope designed by Oldenbourg et al [4], but without the polarization analyzer. Our LC-PolScope is built on the Nikon Eclipse Ti inverted microscope (Nikon Instruments, Melville, New York), with the computer-controlled universal compensator (Hinds Instrumentation, Hillsboro, Oregon)

Biomedical Optics EXPRESS

placed between the interference filter (623 ± 23 nm, Semrock Optics, Rochester, New York) and condenser lens (Fig. 1). Illuminating light is narrowed to 623 nm by the interference filter, and the light is linearly polarized by passing through a universal compensator, allowing for the diattenuation of the sample to be measured. The LC in the universal compensator is controlled by Image J "Micro-manager" software (Vale Laboratory, UCSF) [22] and is automatically rotated to produce polarized light at 0°, 45°, 90° and 135° angles, respective to the horizontal, during image acquisition. The image maps of diattenuation, mean transmittance, and angle of high transmittance are then generated by image analysis algorithms.

Brightfield and fluorescence images are captured using the Nikon DS-U3 camera (Nikon Instruments) and Photometrics CoolSnap MYO camera system (Photometrics, Tucson, Arizona), respectively, under the control of Nikon NIS-Elements AR software (Nikon Instruments). The software allows for multiple fluorescent filters to be readily switched back and forth, and controls the exposure time for each fluorescent filter. Illumination for the fluorescence imaging is generated using the X-Cite 120Q Widefield Fluorescence Microscope Excitation Light Source (Excelitas Technology, Waltham, MA). Light generated from the mercury lamp enters the filter cube, and a dichroic mirror filters this light to the appropriate wavelength, which then passes through the sample. This current set-up allows for the acquisition of polarization, brightfield and fluorescence images of the same sample at the same field of illumination.

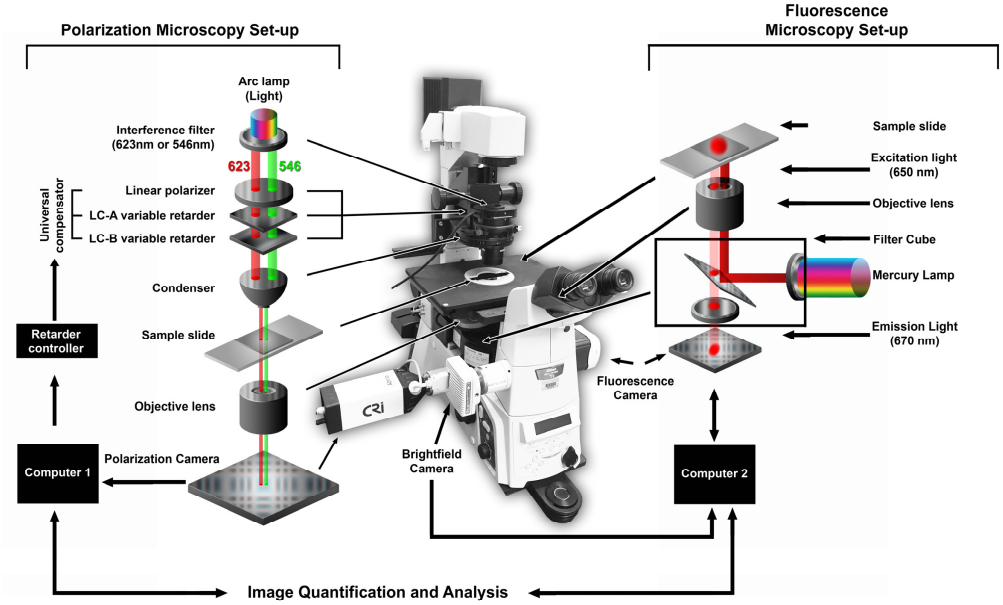

Fig. 1. Schematic diagram of multi-parameter instrument used for live alveolar macrophage diattenuation imaging at 623nm or 546nm wavelengths and fluorescence microscopy. Adapted from Mehta et al. 2013 Journal of Optics [4].

2.5 Calibration of LC-PolScope for diattenuation measurements

Prior to sample analysis, the LC-PolScope was calibrated using a reference standard consisting of a microscope slide comprised of four squares of perfectly polarized glass, oriented at 0, 45, 90, or 135 degrees. The PolScope software utilizes an individual region of interest (ROI) calibration method. In order to calibrate each polarization setting, the glass that is polarized orthogonally to that angle setting was chosen - for example, to calibrate 0° polarized light, an ROI square on the glass oriented 90° relative to the horizontal was

Biomedical Optics EXPRESS

selected. To verify the calibration, a blank region of the slide was visualized, brought out of focus, and a background image was taken. The calibration slide was then visualized and brought back into focus, and a sample image data set of the reference slide standards was generated (Fig. 2(B)-2(E)) and the PolScope measurements were analyzed in relation to the known optical properties of the reference standards. The mean transmittance image map of the slide (Fig. 2(B)) is the average transmittance of each of the four polarization orientations (Fig. 2(E)). As this material is highly anisotropic, each of the four sheets gives a strong diattenuation signal (Fig. 2(C)). The high transmittance angle is measured with respect to the horizontal axis, or in this case, the surface of the slide, and is represented as a pixel intensity value [23]. The angle of high transmittance corresponds to the angle to which the sheet is polarized, i.e. the high transmittance angle of the 0 degree polarized sheet is 0 degrees (Fig. 2(D), top left, yellow square). As previously described, the mean transmittance (Fig. 2(B)), diattenuation (Fig. 2(C)), and high transmittance angle (Fig. 2(D)) image maps are all calculated using the four polarization orientation images (Fig. 2(E)).

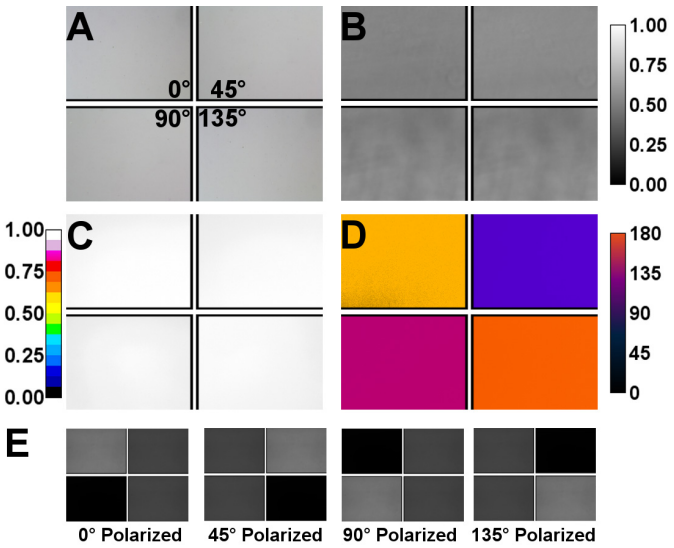

Fig. 2. Calibration of the LC-PolScope instrumentation and software. A slide comprised of four sheets of perfectly polarized glass, with each sheet polarized to light at either 0°, 45°, 90°, or 135° relative to the horizontal is used for calibration. (A) Brightfield image, (B) mean transmittance and (C) diattenuation image map of the calibration slide. (D) Colored schematic representing the angle of high transmittance, or the orientation of light which is most transmitted by the object. (E) Images generated from passing linearly polarized light at 0°, 45°, 90°, and 135°, from left to right, which are used to calculate the angle of high transmittance, diattenuation, and mean transmittance image maps.

2.6 Multi-parameter image acquisition of isolated CLDIs and alveolar macrophages

Isolated CLDIs and alveolar macrophage samples were imaged using a 40x objective lens. The LC-PolScope was used to capture the linear diattenuation of the sample using a 623 ± 23 nm interference filter (Semrock Optics, Rochester, New York). Once the polarized light images were captured, the filter and universal compensator were removed, and the color camera was used to take a brightfield image of the sample. The fluorescence camera was then used to assess the fluorescent properties of the sample, using a standard Cy5 filter set.

2.7 Multi-parameter cytometric image analysis

All images generated using the LC-PolScope software were analyzed using ImageJ [24–26]. These images are 8-bit images, yielding intensity values from 0 to 255. The values for diattenuation, mean transmittance, and fluorescence are obtained by extracting the pixel

Biomedical Optics EXPRESS

values from the image maps at exact locations, denoted as (x,y) coordinates. Each pixel will have an intensity value *z* associated with it, located such that 1≤x≤X and 1≤y≤Y, where X and Y define the total dimensions of the image such that the resolution of the image is defined as R = X*Y. The image maps generated represent the values of diattenuation, mean transmittance, and Cy5 fluorescence as such:

Diattenuation: $D_\lambda(x,y)$ is the diattenuation signal at wavelength λ for the pixel located at (x,y) Mean Transmittance: $T_{M,\lambda}(x,y)$ is the mean transmittance at wavelength λ for the pixel located at (x,y) Fluorescence: $F_{Cy5}(x,y)$ is the Cy5 fluorescence of the pixel located at (x,y)

To compare the diattenuation, optical density, and Cy5 fluorescence of cells at a whole cell level, an automated data acquisition strategy was put in place, and is summarized in Fig. 3. First, the zero-degree polarization state image was selected (Fig. 3, Panel A), and the brightness and contrast are manually adjusted to allow for cells to stand out from the well-plate background (Fig. 3, Panel B). Following this, the adjusted image was then subjected to a manual thresholding, which generates a binary mask to discriminate between objects and background (Fig. 3, Panel C). The binary mask was then subjected to the "Fill Holes" function in ImageJ, which fills holes within each object, allowing for a more complete cellular mask to be generated (Fig. 3, Panel D). Once the mask has been generated, the dichroism, mean transmittance, and fluorescence image maps for a single field of view were opened and the cells in the image were analyzed using the "Analyze Particles" function within ImageJ, and, using the previously generated binary image as a mask, a region of interest (ROI) was selected to analyze the pixels contained within the cell, and is denoted as p(c). The objects across each image were analyzed, with objects greater than 250 pixels^2 in area being selected for, measuring the total, integrated signal intensity of diattenuation, mean transmittance, and Cy5 fluorescence for the same cell 'c' in the following manner:

$$D_\lambda(c) = \sum_{(x,y)\in p(c)} D_\lambda(x,y) \tag{1}$$

$$T_{m,\lambda}(c) = \sum_{(x,y)\in p(c)} T_{m,\lambda}(x,y) \tag{2}$$

$$F_{Cy5}(c) = \sum_{(x,y)\in p(c)} F_{Cy5}(x,y) \tag{3}$$

The integrated optical density (OD) of the drug crystals was determined using the integrated mean transmittance as follows:

$$OD_\lambda(c) = \sum_{(x,y)\in p(c)} -\log 10(T_{m,\lambda}(x,y)) \tag{4}$$

To correct for background signal, the integrated OD was corrected by subtracting the average integrated background optical density as follows:

$$OD_\lambda(c) = \sum_{(x,y)\in p(c)} -\log 10(T_{m,\lambda}(x,y)) - \sum_{(x,y)\in p(c)} -\log 10(T_{M,\lambda}(BG)) \tag{5}$$

To obtain the average diattenuation, optical density, or Cy5 fluorescence within an object of interest, the values obtained from Eqs. (1), (3), and (5) are divided by the total area analyzed, as such:

$$\bar{D}_\lambda(c) = \frac{\sum_{(x,y)\in p(c)} D_\lambda(x,y)}{A} \tag{6}$$

$$\bar{OD}_\lambda(c) = \frac{\sum_{(x,y)\in p(c)} -\log 10(T_{m,\lambda}(x,y)) - \sum_{(x,y)\in p(c)} -\log 10(T_{M,\lambda}(BG))}{A} \tag{7}$$

$$\bar{F}_{Cy5}(c) = \frac{\sum_{(x,y)\in p(c)} F_{Cy5}(x,y)}{A} \tag{8}$$

Biomedical Optics EXPRESS

All average values are reported on a 0-1 scale by dividing by 255. All integrated signal values are reported as the total signal value, with each individual pixel ranging from 0 to 255.

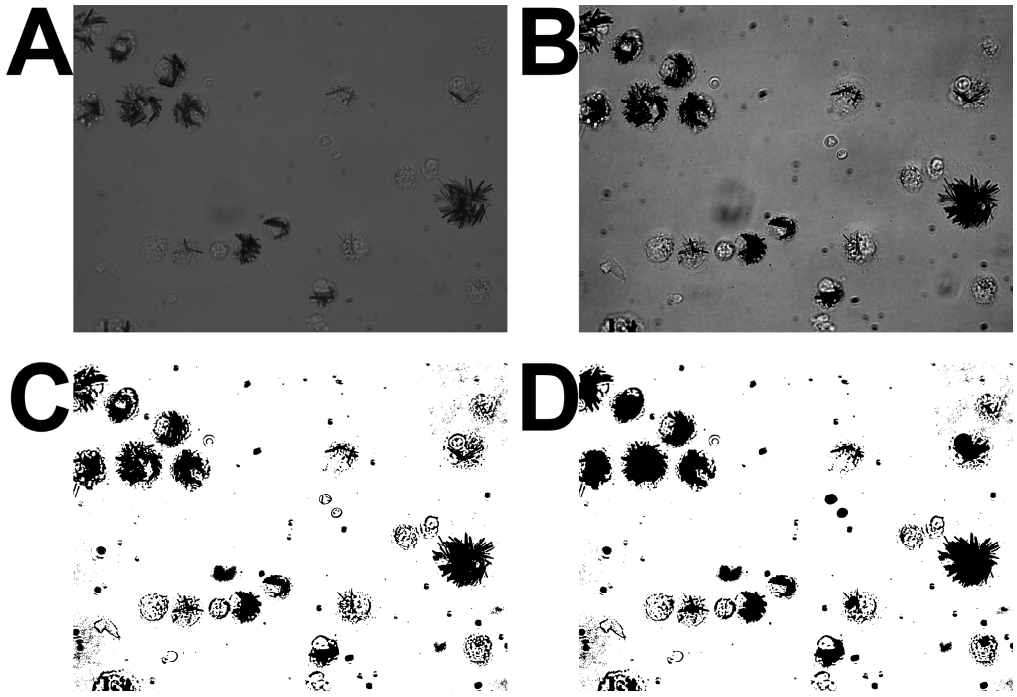

Fig. 3. Representative schematic of mask generation for data collection. The 0-degree polarization state image is selected (Panel A) and has the brightness and contrast adjusted (Panel B). Following this, the image undergoes a manual threshold in ImageJ, delineating between objects and background (Panel C). The image then undergoes the "Fill Holes" function, generating the mask for data analysis (Panel D)

2.8 Statistical analysis

Statistical tests were performed with IBM SPSS Statistics version 24.0 (IBM Software, Armonk, New York). Results are reported as average ± standard deviation. P values less than 0.05 were considered statistically significant.

3. Results

3.1 Imaging and quantification of diattenuation, optical density, and Cy5 fluorescence of CLDIs using multi-parameter imaging system

To demonstrate the capabilities of this multi-parameter imaging system, the drug clofazimine was chosen as a model compound. Clofazimine (CFZ) is a bright red phenazine drug that accumulates extensively in tissues throughout the organism, leading to the formation of deep red, crystal-like drug inclusions *in vivo* [27]. Following eight weeks of CFZ treatment, CLDIs were isolated from the spleen of a mouse and imaged with the polarization and fluorescence imaging system. These CLDIs are deep red, and have a rod-like polygonal shape, with an average size of 17.6 ± 10.9 μm^2 (Fig. 4(A)). These crystals strongly absorbed linearly polarized light of 623 nm wavelength, and had an average optical density (OD) of 0.31 ± 0.12 (Fig. 4(B)). Interestingly, CLDIs are able to interact with different orientation states of polarized light, resulting in a strong diattenuation signal. As a result of the crystallinity and molecular order present in the CLDI, different orientations of polarized light are absorbed to different extents by the crystal, yielding an average diattenuation signal of 0.26 ± 0.05 (Fig. 4(C)). The CLDIs are also highly fluorescent in the Cy5 channel (excitation/emission), which

Biomedical Optics EXPRESS

occurs due to the formation of a mono-protonated, hydrochloride salt during the process of clofazimine accumulation and biocrystallization [20] (Fig. 4(D)). The crystals had an average Cy5 fluorescence of 0.06 ± 0.02. After analyzing isolated CLDIs from mice treated with CFZ, we decided to probe the utility of this instrument in studying live cells isolated from animals fed the drug for a period of eight weeks.

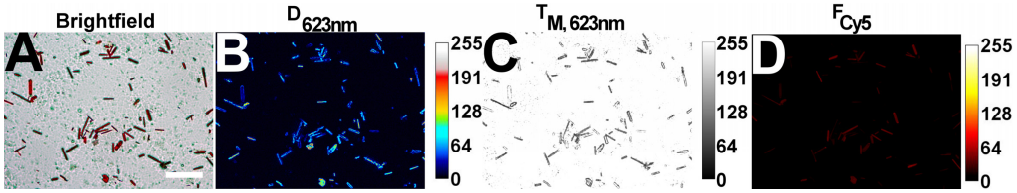

Fig. 4. Pol-Scope images of CLDIs isolated from the spleen of 8wk CFZ-treated mice. (A) Brightfield image displaying deep red color, rod-like shape of CLDIs. (B) Diattenuation, (C) mean transmittance and (D) Cy5 fluorescence of CLDIs with illuminating light at 623 nm. The high degree of diattenuation and Cy5 fluorescence of the CLDIs is readily visible. Scale bar is 50 μm.

3.2 Multi-parameter live cell imaging and quantification of diattenuation, optical density, and fluorescence of drug-treated alveolar macrophages

Based off of previous work, it has been shown that CLDIs tend to be found within tissue macrophages, such as Kupffer cells of the liver, red pulp macrophages of the spleen, and alveolar macrophages within the lung [18, 28, 29]. Due to the extensive accumulation within alveolar macrophages, these cells were chosen to test this multi-parameter imaging and analysis system in live cells. These cells serve as the first barrier to incoming airborne pathogens and other inhaled xenobiotics, and have been shown to be greatly impacted by the accumulation of these materials [30]. Alveolar macrophages were isolated from mice treated with CFZ for eight weeks or mice fed a control diet, and imaged using the combined polarization and fluorescence imaging system.

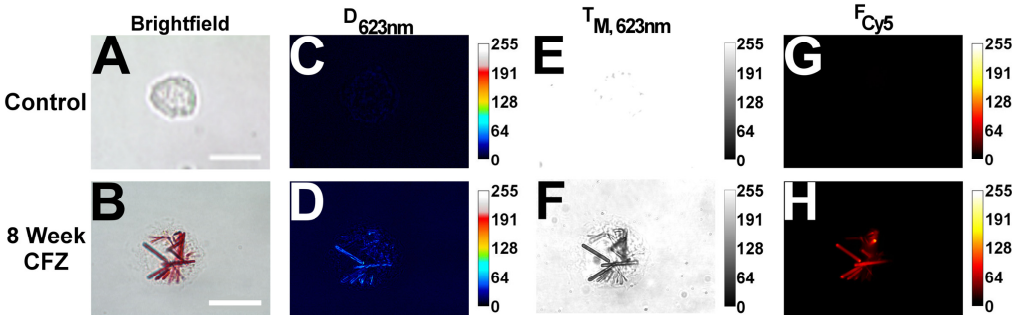

Fig. 5. Comparison of CFZ treated and control alveolar macrophages. Macrophages from mice following 8 weeks of treatment, displayed the characteristic CLDI formation. Brightfield (A, B), diattenuation (C, D), mean transmittance (E, F), and Cy5 fluorescence (G,H) images of isolated alveolar macrophages from treated and non-treated (control) mice. Both diattenuation and mean transmittance images were generated using illuminating light at 623nm. Note that the diattenuation and mean transmittance signal is entirely contained within the CLDIs. Scale bar is 15 μm.

Upon visual inspection of the brightfield image, control diet-fed macrophages are small, rounded cells, ranging in size from 10 to 25 microns in diameter. Imaging of these cells using the multi-parameter imaging system revealed a low, but detectable, dichroism signal of 0.018 ± 0.005 (Table 1). This signal arises due to interactions of the polarized light with cellular components, such as membranes and organelles, which have some degree of molecular organization. The mean transmittance image shows cells with very low optical density, with an average intensity of 0.021 ± 0.029.These cells are, by and large, transparent, with

Biomedical Optics EXPRESS

occasional dark spots, which may correspond to cellular components, such as lysosomes or other membrane-bound organelles. Control alveolar macrophages show little to no fluorescence in the Cy5 channel, as is expected (0.0002 ± 0.00005). Representative images of the untreated alveolar macrophages are seen in Fig. 5, top panel.

Following eight weeks of sustained therapy with CFZ, the alveolar macrophages are loaded with large amounts of intracellular crystals of the drug, consistent with previous reports from our laboratory [29]. As a result of the accumulation of intracellular drug complexes, intracellular dichroism increased significantly (0.042 ± 0.013, $p<0.01$, Two-Tailed Student's T-Test), revealing that CLDIs are highly organized, self-assembling supra-molecular entities, and that the dichroism of these crystals can be detected within a cell. CLDI accumulation and formation also resulted in a significant increase in the optical density of the macrophages (0.054 ± 0.071, $p<0.01$, Two-Tailed Student's T-Test), as a result of the deep red color associated with these biocrystals. Consistent with previous reports [20], CLDI accumulation also resulted in a concomitant increase in the Cy5 fluorescence associated with the macrophages as well (0.012 ± 0.019, $p<0.01$, Two-Tailed Student's T-Test).

Table 1. Average Signal Intensity of Macrophages

	Control Alveolar Macrophage (n=215)	8 Week CFZ Fed Alveolar Macrophage (n=201)
$\overline{D_{623}}$	0.017 ± 0.004	0.042 ± 0.013 *
$\overline{OD_{623}}$	0.017 ± 0.019	0.054 ± 0.071 *
$\overline{F_{Cy5}}$	0.0002 ± 0.00004	0.012 ± 0.019 *

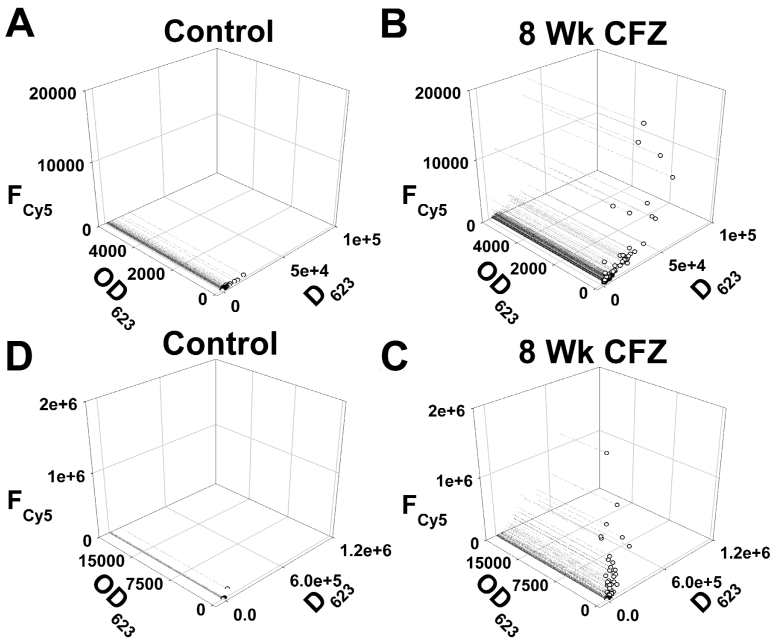

Fig. 6. Scatter plot displaying relationship between Cy5 fluorescence, optical density, and dichroism in control alveolar macrophage populations (A, D) and 8 week CFZ fed alveolar macrophage populations (B,C). Panels A and B show the same population of cells shown in panels D and C, but zoomed into the lower signal values. Treatment with CFZ results in a heterogeneous population of macrophages on basis of optical signals, while untreated cells remain homogenous.

The analyses performed also studied how each of these three properties related to one another in both control and CFZ-treated cells. By plotting the total integrated dichroism,

Biomedical Optics EXPRESS

optical density, and fluorescence of the cells, one can gain further understanding on how the molecular order (represented by dichroism), degree of accumulation (represented by optical density), and protonation state (represented by fluorescence) of the drug relate to one another following eight weeks of sustained therapy. Performing this analysis also allows for the study of the optical properties of an entire population of cells to be observed, which can be a useful analysis when determining how different cell populations accumulate drugs both *in vitro* and *in vivo*. Figure 6 compares the optical properties from both control alveolar macrophages (A, D) and those from a mouse fed 8 weeks (B, C). In Panel A, one can see that, on a whole population level, these cells display very low fluorescence and optical density, with a more varied dichroism signal. In all, the control cells display little variability with respect to their optical signals, and this is captured in the plots shown in Panels A and D. On the other hand, treatment with CFZ, and the subsequent accumulation and biocrystal formation which occurs as a result, causes there to be three populations of cells which can be segregated. In Panel B, there is a population of cells aggregated very near the origin, showing low fluorescence, optical density, and dichroism. These cells are most likely red blood cells which were not eliminated during the collection and plating of the macrophages. The second population of cells shows an elevated fluorescence, optical density, and dichroism compared to the previously described population; these cells are most likely macrophages which have accumulated soluble CFZ, but have not yet formed a CLDI (Panel B). The final population of cells can be seen in Panel C. These cells display very high fluorescence, optical density, and dichroism, indicating that these cells are most likely alveolar macrophages which contain at least one intracellular crystal.

4. Discussion

The development and refinement of polarized light microscopy measurements to study changes in the organization of molecular components in individual cells has had many applications in cell biology and beyond [4, 31, 32]. To study the bioaccumulation of small molecule drugs inside cells, the experiments presented here indicate how a quantitative multi-parameter imaging system combining polarization, transmittance and fluorescence measurements can be useful for studying the cellular mechanisms of drug disposition from the cellular to the molecular level. Previously, our lab has used polarization microscopy to study the optical properties of drug inclusions formed *in vitro*. Cells were incubated with CFZ and other phenazine derivatives to study the self-assembly of drug aggregates in live cells, revealing that, even after 72 hours, the self-assembly of CFZ aggregates within cells yields a measurable diattenuation signal [33]. Cultured cells, however, are not the optimal model for studying intracellular drug crystallization for a variety of factors, namely the length of time necessary for the crystals to form. Thus, a long term *in vivo* study was performed to develop a method to accurately quantify changes in intracellular dichroism, absorbance, and fluorescence induced following eight weeks of CFZ therapy.

Through the development of this multi-parameter imaging and analysis system, drug accumulation, as well as the changes this accumulation has within the cell with respect to molecular order can be studied at the level of single cells in a rapid manner. Further applications of this instrument can potentially be used to study large populations of cells which can allow for researchers to discriminate which cells have a propensity to accumulate and sequester soluble drug, or potentially form an insoluble aggregate. Due to the automated nature of the analysis, all of the objects analyzed may not be macrophages, but rather red blood cells or other immune cells, such as B cells. However, by analyzing each of the three cellular properties measured using this method, one can place each cell in a category on the basis of the intensity of the signals measured. For example, cells which display a high level of fluorescence, dichroism, and optical density are most likely macrophages containing an intracellular crystal. Red blood cells, on the other hand, would show low levels of fluorescence and optical density. Further refinement of the imaging and analysis technique

Biomedical Optics EXPRESS

can be used to rapidly image and analyze large populations of live cells from drug treated animals, allowing for investigators to determine how, if at all, various drugs accumulate within these cells without the need for time-consuming chemical analyses.

Previously, we have characterized the molecular organization and chemical composition of CLDIs following biochemical isolation, using nuclear magnetic resonance, powder X-ray diffraction, transmitted electron microscopy, freeze fracture electron microscopy, liquid chromatography and mass spectrometry [18, 19, 34]. Our results demonstrated that CLDIs are comprised of subdomains of pure CFZ-hydrochloride crystals [34], bounded by multilamellar membrane structure of biological origin [18, 19]. Consistent with these previous results, quantitative polarization microscopy revealed the manner in which microscopic domains of ordered CFZ molecules within CLDIs of live macrophages obtained from CFZ-treated mice differentially interact with polarized light. Nevertheless, unlike the aforementioned chemical analysis techniques, quantitative multi-parameter observations were performed on functional, viable cells.

In terms of its implications for drug targeting and delivery, the formation and fate of intracellular drug biocrystals has remained a poorly understood aspect of pharmacokinetics, precisely because of the lack of practical, quantitative techniques to study intracellular drug bioaccumulation. Nevertheless, understanding the mechanisms responsible for the accumulation of drugs within intracellular compartments is important as it may explain why some drugs fail to reach proper therapeutic concentrations at a site of action or to explain unfavorable drug-drug interactions that may occur through bioaccumulation dependent pathways [35]. Drug trapping and accumulation can lead to alterations in the structure and function of organelles, affecting cell physiology [36]. Accumulation of small molecule drugs in organs such as the liver and kidney are particularly concerning as a potential cause of toxicity [37, 38]. For example, the antiviral drug cidofovir (Gilead Sciences) tends to accumulate in the kidneys, leading to nephrotoxicity [39]. Yet, there are also specific cases in which drug bioaccumulation may be beneficial. Many of the anti-malarial drugs in the 4-aminoquinolone class have been shown to be more effective in treating the illness due to preferential accumulation within an acidic compartment of the parasite [40, 41].

The development and refinement of a multi-parameter imaging system which combines polarization and fluorescence microscopy may further the understanding of intracellular drug bioaccumulation via the mechanism of CLDI formation in macrophages and potentially other cell types. In addition to CLDIs formed by clofazimine, this quantitative multi-parameter imaging set up could be used to detect ordered molecular aggregates formed inside cells by other drugs. Imaging systems such as this can also be applied in drug discovery: by looking for drugs which induce similar changes in intracellular molecular organization, drugs that potentially crystallize intracellularly can be identified as potential target molecules for therapeutics. While CFZ and CLDIs are deeply red and fluorescent, other drugs which accumulate may not be as easy to detect with the naked eye. Through the use of polarization microscopy, minute changes in the underlying structure which may be induced by drug accumulation can potentially be detected; this may provide information about the subcellular localization of drug. Indeed, much remains to be discovered about the physiological function of xenobiotic sequestering macrophages, and the underlying biological mechanisms responsible for CLDI formation. Furthermore, beyond the study of drug transport phenomena, a quantitative multi-parameter imaging set up could also be used for studying many other kinds of phenomena associated with the formation of ordered molecular aggregates, such as the formation of hemoglobin crystals in sickled red blood cells [42]; the formation of atherosclerotic plaques [43]; the formation of misfolded protein fibrils as seen in Parkinson's and Alzheimer's disease and other forms of dementia [44, 45]; and the formation of lipid aggregates as is characteristic of certain lysosomal storage diseases [46].

Biomedical Optics EXPRESS

5. Conclusion

To conclude, this research describes how a quantitative, fluorescence-transmittance-polarization multi-parameter imaging system can be used for detecting and studying CLDIs in isolation, as well as studying the accumulation of drug in live macrophages obtained from drug treated animals at differing stages in treatment. CLDI formation leads to the development of a highly organized molecular structure that homogenously interacts with linearly polarized light. While all experiments reported herein were performed with alveolar macrophages, other macrophage populations, such as those in the spleen, liver, bone marrow and in the peritoneal cavity have been previously implicated in the disposition of clofazimine, and should also be amenable for comparative analysis. In the future, establishing how the optical properties of CLDIs vary amongst different macrophage populations, as a function of clofazimine dose, and in mouse mutants harboring mutations that affect macrophage function, will be especially useful to elucidate the molecular mechanisms driving the pharmacokinetics of clofazimine accumulation.

Acknowledgments

The authors would like to thank Rudolf Oldenbourg and Grant Harris for help with the LC-Polscope and associated image analysis algorithms. This work was funded by NIH grant R01GM078200 to GRR